Extension and slip rate partitioning in NW Iran constrained by GPS measurements Research article

A. Rastbood^{1*}, B. Voosoghi¹

1 Department of Geodesy Engineering, Faculty of Geodesy and geomatics Engineering, K.N.Toosi University of Technology, Tehran, Iran

Abstract:

Convergence of $22\pm 2~{\rm mm\,yr^{-1}}$ between the northward motion of the Arabian Plate relative to Eurasia at N8° $\pm 5^{\circ}$ E is accommodated by a combination of thrust and strike-slip faults in different parts of Iran. Dislocation modeling is used to examine the GPS data for this part of the Alpine-Himalayan mountain belt with more concentration in NW Iran. First, the vectors due to known Arabia-Eurasia rotation are reproduced by introducing structures that approximate the large-scale tectonics of the Middle East. Observed features of the smaller scale fault system are then progressively included in the model. Slip rate amplitudes and directions adjusted to fit available GPS data. Geological evidences show strike-slip and reverse-slip faulting in NW Iran, but GPS data show normal faults in this region too. By slip partitioning we propose four locations for normal faults based on extensions observed by GPS data. Slip rate values were estimated between 2 ~ 5 mm/yr for proposed normal faults. Our modeling results prove that the NW Iran is not only affected by Arabia-Eurasia collision but also contributes in the subduction motion of the South Caspian and Kura basins basement beneath the Apsheron-Balkhan sill and the Great Caucasus respectively.

Keywords:

Arabia-Eurasia collision • GPS velocity field • extension • dislocation theory • interseismic deformation • slip partitioning • tectonics © Versita sp. z o.o.

Received 28-04-2011; accepted 17-08-2011

1. Introduction

It was recognized early in the development of plate tectonics that plate boundaries in continental areas are substantially wider than those in oceanic plates (Isacks et al., 1968; McKenzie, 1970; Molnar and Tapponnier, 1975). Arabia-Eurasia oblique collision zone is such an area.

The surface deformations over long periods of time (Quaternary and Miocene) appear localized on the major fault systems. It occurs first in an earthquake. Total geological offset produced by a fault is derived from the sum of co-seismic offsets. Unfortunately, major earthquakes are rare, their return period are around e.g. 1800-2100, 500-800, and 850-950 years in the study region (Berberian and Yeats, 2001). Since the recording of seismic waves are

hardly more than one hundred years, any attempt to quantify the deformation by integrating the co-seismic deformation is unreliable. So attempts to estimate the surface deformation by summing the contributions of co-seismic deformation result in deformation rates inconsistent with long-term rates (Jackson et al., 1995). Moreover the method of summation of the seismic moments diffuses and smoothes the deformation which can not be attributed to active faults but supposed to the continuous deformation of the lower crust and the upper mantle(Kostrov, 1974). Thus seismicity does not make it possible to quantify the deformation. However seismicity and focal mechanism solutions in the study area (Figure 2(b)) provide primary qualitative information to constrain the style of slip accommodated by a fault activity.

The global positioning system (GPS) is an important tool to quantify continental deformation to a precision and on a scale unprecedented in the Earth Sciences (Hager et al., 1991). Over the last decade numerous campaigns and recently continuous GPS sites have been established throughout Iran resulting in progressively

^{*}E-mail: arastbood@dena.kntu.ac.ir



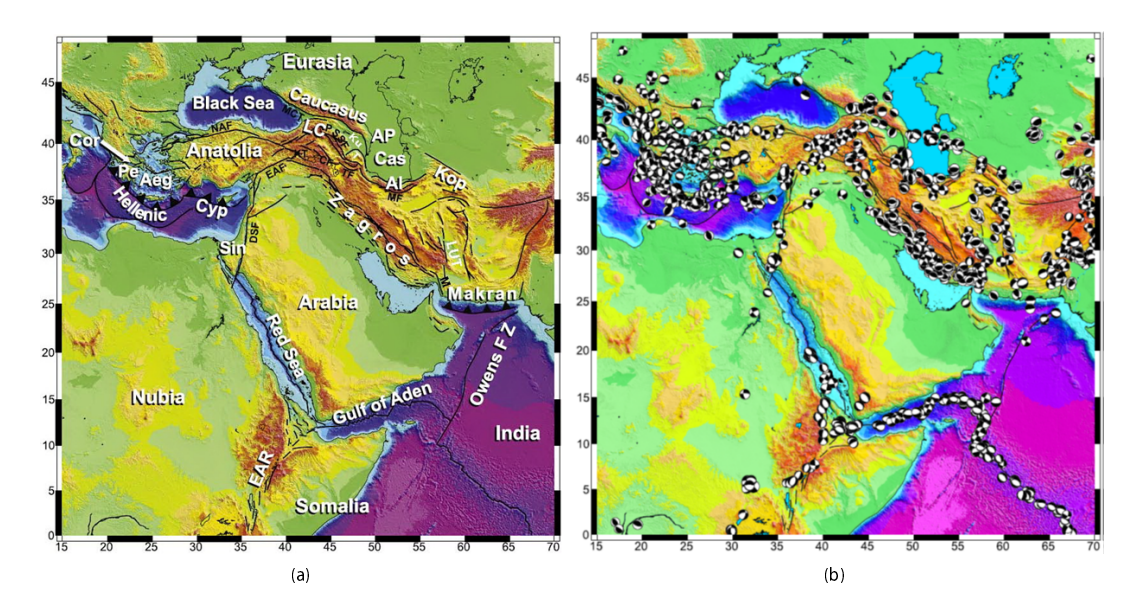


Figure 1. (a) Simplified topographic/bathymetric (SRTM30 PLUS; httml) and tectonic map of the study area, including the zone of interaction of the Nubian, Somalian, Arabian, and Eurasian plates. Abbreviations are North Anatolian fault (NAF), East Anatolian fault (EAF), Dead Sea fault (DSF), Talesh Mountains (T), Mosha fault (MF), Pembak-Sevan-Sunik fault (PSSF), Tabriz fault (TF), Chalderan fault (CF), Gulf of Corinth (Cor), Peloponnesus (Pe), Aegean (Aeg), Lesser Caucasus (LC), Cyprus trench (Cyp), Karliova Triple junction (KT), Kura basin (Ku), Sinai (Sin), Caspian basin (Cas), Main Caucasus Thrust (MCT), East African rift (EAR), Kopet-Dag (Kop), Lut Block (LUT), Minab-Zandan-Palami fault (M), Apsheron-Balkhan sill (AP), Alborz Mountains (Al). Modified after Reilinger et al. (2006). (b) Focal mechanisms for earthquakes in the study area (lower hemisphere projections) from Harvard catalog, 1976 to January 2005 used as con. Base map is as in Figure 2(a). After Reilinger et al. (2006).

better determination of the velocity vectors describing interseismic crustal deformation for this part of the Alpine-Himalayan mountain belt (Bayer et al., 2006; Djamour et al., 2010; Djamour et al., 2011; Hessami et al., 2006; Masson et al., 2007; Masson et al., 2006; McClusky et al., 2000; McClusky et al., 2003; Nilforoushan et al., 2003; Peyret et al., 2009; Reilinger et al., 2006; Vernant et al., 2004a; Vernant et al., 2004b).

Such deformation can now be compared with rates determined by geological and geomorphic methods over longer time periods (Allen et al., 2003; Bachmanov et al., 2004; Jackson et al., 2006; Nankali, 2011; Reilinger et al., 2006; Talebian and Jackson, 2002; Tavakoli et al., 2008; Vernant and Chéry, 2006; Vernant et al., 2004a; Walker and Jackson, 2002, 2004; Walker and Jackson, 2006, 2006; Walker and Jackson, 2002, 2004; Walker and Jackson, 2006, 2006; Walker and Jackson, 2002, 2004; Walker and Jackson, 2006, 2006; Walker and Jackson, 2006, 2006; Walker and Jackson, 2006, 2006; Walker and Jackson, 2006; Walker and Jackson, 2006, 2006; Walker and 2006, 2006; Walker and 2006, 2006; Walker and 2006; Walker and 2006, 2006; Walker and 2006; Walker and 2006, 2006; Walker and 2006, 2006; Walker and 200

Although this paper concentrates in NW Iran, we begin by creating a large-scale model that incorporates the major active structures and reproduce the results (including defects) of using a simple Arabia-Eurasia pole of rotation in the Middle East (Djamour et al., 2010; Vernant et al., 2004b). Within the context of this model, velocity vectors are then examined using a knowledge of the faults with known Quaternary activity (Bachmanov et al., 2004; Copley and Jackson, 2006; Stocklin, 1968; Walker and Jackson, 2004). This is done with more details in NW Iran based on GPS data. This part of Iran has excited interests because of destructive historical earthquakes (Ambraseys and Melville, 1982). Further destructive events are to be expected in the future (Djamour et al., 2011).

Recent modeling approaches have assumed that geological structures divide a region into blocks and use procedures that minimize strains within them (McClusky et al., 2001; Meade et al., 2002; Reilinger et al., 2006). These procedures however, can result in motion on a structure being incompatible with surface observations (e.g. closure on an extensional feature). Our model does not require the closed undeforming blocks, but requires that the direction of the horizontal component of slip vectors on the structures that we model are compatible with geological and seismological observations (Canitez, 1969; Chandra, 1984; Hessami and Jamali, 2006). The significance of deformation within blocks is discussed by Hubert-Ferrari et al. (2003).

Based on observed extensions in NW Iran by Masson et al. (2006) we determine four locations for probable normal faults with slip rates between 2 ~ 5 mm/yr in these extensional regions. Using slip partitioning with more details we get a more precise tectonic model for the NW Iran. Our model explains the reason of extension observed in this region. It shows that this part of Iran is not only affected by Arabia-Eurasia collision but also contributes in the subduction motion of the South Caspian and Kura basins basement beneath the Apsheron-Balkhan sill and the Great Caucasus respectively.



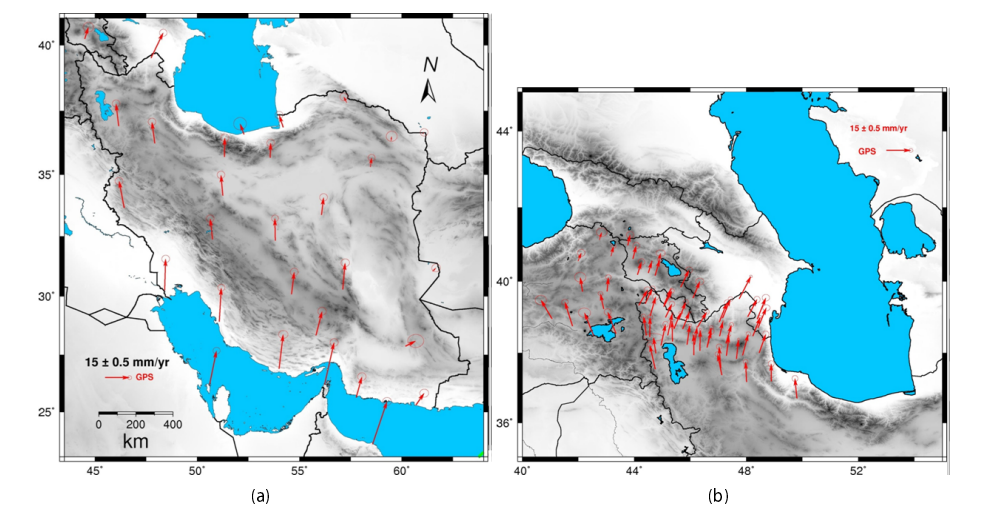


Figure 2. GPS velocities relative to Eurasia record 22±2 mm yr⁻¹ N–S shortening between Arabia–Eurasia, which is accommodated throughout Iran. (a) GPS velocity vectors of campaign global geodynamic network of Iran used for large-scale and detailed modeling in Iran from Reilinger et al. (2006). (b) Eurasia fixed GPS velocity vectors of campaign and continuous local geodynamic networks in NW Iran from Djamour et al. (2011) used to continue the detailed modeling in NW Iran.

2. The tectonic framework

Iran in the boundary between Arabia and Eurasia (Figure 1) is an ideal laboratory for studying the kinematics of plate interactions because of the various tectonic processes encountered, including continental collision (Zagros, Caucasus, Alborz, Kopet-Dag, Talesh), subduction of oceanic lithosphere (Makran) and a sharp transition between a young orogen (Zagros) and a subduction zone (Makran). The geodynamics of the region is dominated by the convergence between the Arabia and Eurasia plates (Jackson and McKenzie, 1984, 1988).

The Arabia-Eurasia convergence takes place first in southern Iran with the Zagros fold and thrust belt (Figure 2(a)) that started as early as late Eocene (Hessami et al., 2001). However, the climax of orogeny indicated by the Alborz and Zagros uplift and South Caspian subsidence took place during the late Neogene subsequent to the complete closure of the Neo-Tethyan ocean (Alavi, 1994; Berberian et al., 1982; Berberian, 1983, 1995; Falcon, 1974; Stocklin, 1968). Compressional structures in this range are striking obliquely to the convergence direction (especially in the central and northern part). This is probably due to partitioning between thrusting and strike-slip on major faults such as the Main Recent Fault in northern Zagros (Jackson, 1992; Talebian and Jackson, 2002). North of Zagros, the Central Iranian Block is believed to be rigid (Jackson and McKenzie, 1984), and part of the deformation is transmitted to the north in the Alborz, Talesh and Caucasus Mountains (Figure 2(a)). The Alborz and Talesh Mountains are surrounding the western and southern border of the South Caspian Block. The regular occurrence of large historical earthquakes in Alborz suggests an important deformation of this mountain belt north of Tehran. East of South Caspian basin, the Kopet-Dag is accommodating part of the Arabia-Eurasia convergence not absorbed by the Makran subduction. South of the Kopet-Dag belt, the Lut Block is bordered to the west and east by large strike slip faults (Nowroozi and Mohajer-Ashjai, 1985; Tirrul et al., 1983; Walker and Jackson, 2002). Large strike-slip motion is also reported along the Minab-Zandan-Palamifault zone that corresponds to the transition zone between the Zagros collision and Makran subduction (Falcon, 1976; Haynes and McQuillan, 1974; Kadinsky-Cade and Barazangi, 1982).

The north component of the GPS velocity field expressed in a Eurasian reference frame decreases from the Persian Gulf in the south to the Caspian basin in the north. In NW Iran, this simple sketch fails: velocity increases north of Central Iranian Block up to the Kura basin in Azerbaijan (Figure 3(a) and 3(b)). Geodetic motion suggests a prominent N30° E extension to the Tabriz fault where compression would be expected. GPS data shows also two zones of extension, one just north of Tabriz fault in the south of the Talesh plateau and another close from Azerbaijan border north of Talesh plateau. This intriguing feature may either indicate that the tectonic of this region is not simply driven by the Arabian indenter or that a transient motion is occurring (Masson et al., 2006).

3. Modeling approach

Most of GPS velocity vectors relative to Eurasia can be explained by rotation of Arabia around an euler pole relative to Eurasia. However, most GPS sites show misfits that fall outside the errors of observation. Our modeling approach solves this problem. It is described by Flerit et al. (2003) and Armijo et al. (2004).



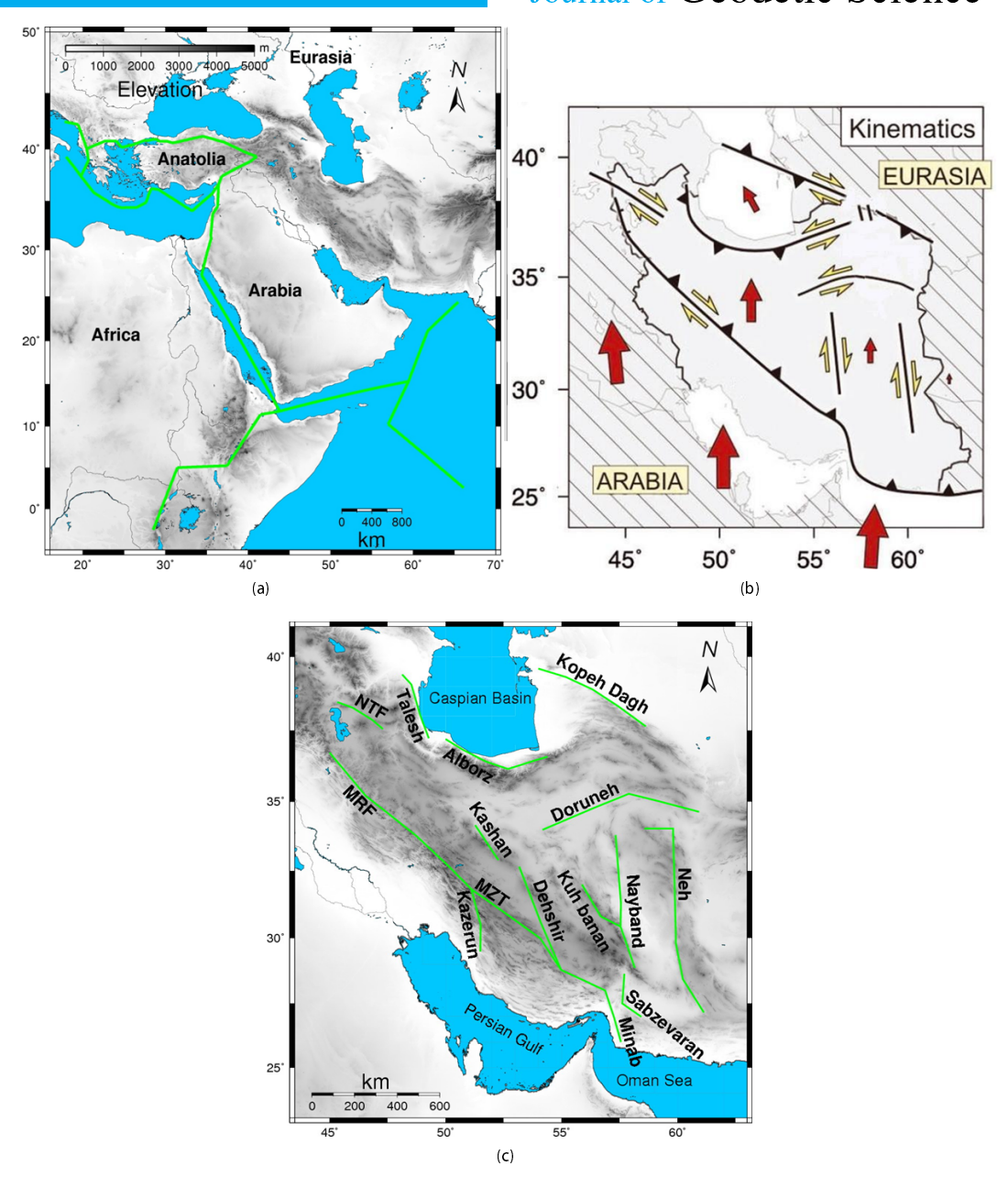


Figure 3. (a) The initial large-scale model elements (in green) reproducing the overall Arabia/Eurasia kinematics. (b) Schematic summary map showing the present day tectonic setting and kinematics of Iran in the Arabia and Eurasia convergence region. Red arrows, indicating motions relative to Eurasia, show approximately how N–S shortening is accommodated across the region. Black lines show the nature of deformation across major fault zones. Yellow arrows indicate the sense of slip for strike-slip faults. Modified after Hollingsworth et al. (2010). (c) Selected elements (in green) based on major active faults for detailed modeling in Iran.

Dislocation theory can be described as that part of the theory of elasticity dealing with surfaces across which the displacement field is discontinuous. The elastic dislocation formulation of Okada (1985) was used in our modeling, which expresses the displacement field at any given point as a function of fault geometrical parameters (slip rate, locking depth, dip, length and width) and the

elastic constants of the medium (Lame coefficients). The Okada (1985) formulation is mathematically robust and tractable, and these attributes make it suitable for rapid forward modeling.

As commonly done in mathematical physics, it is necessary for simplicity to make some assumptions. Here the curvature of the earth, its gravity, temperature, magnetism and non-homogeneity



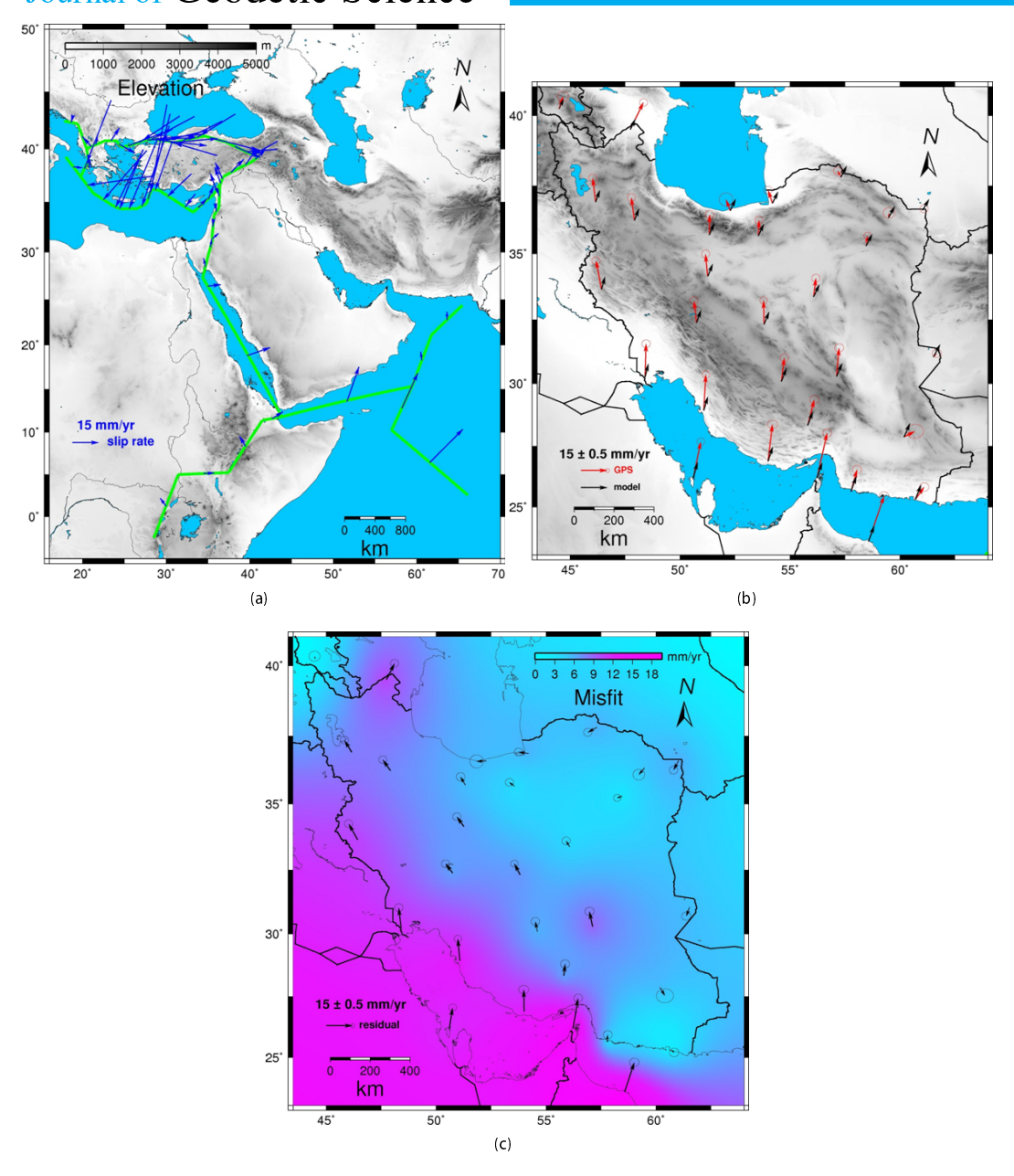


Figure 4. Large-scale modeling. (a) Inter-plate elements (in green) of the Middle East, i.e., the faults between Arabian, Nubian, Somalian, Indian plates and around Anatolia plateau modelled together to reproduce the large-scale velocity field in Iran. (b) Selected GPS velocity field (in red) from Reilinger et al. (2006) with 95% confidence ellipses together with initial model velocity field (in black). The large-scale model is only approximate for Iran. (c) Residual vectors (in black) plus shading (in red) indicating the degree of misfit. It's calculated by interpolating between scalar values of the misfit. Large residuals are visible southwest of Iran parallel and perpendicular to oblique collision zone of Arabia and Eurasia plates.

are neglected and a semi-infinite medium which is homogeneous and isotropic is considered. For our modeling, the geometrical fault parameters are constant for each fault segment (element) and displacements are calculated at each point on the free surface.

For most faults in the model, the GPS coverage is not sufficiently

dense near the faults to provide good constraints on fault locking depths. This adds an uncertainty to model slip rates because there is a trade-off between locking depth and slip rate (slip rate increases with locking depth) (Meade and Hager, 2005). This trade-off occurs because GPS velocities near a locked fault will have smaller velocities than those far from the fault due to the



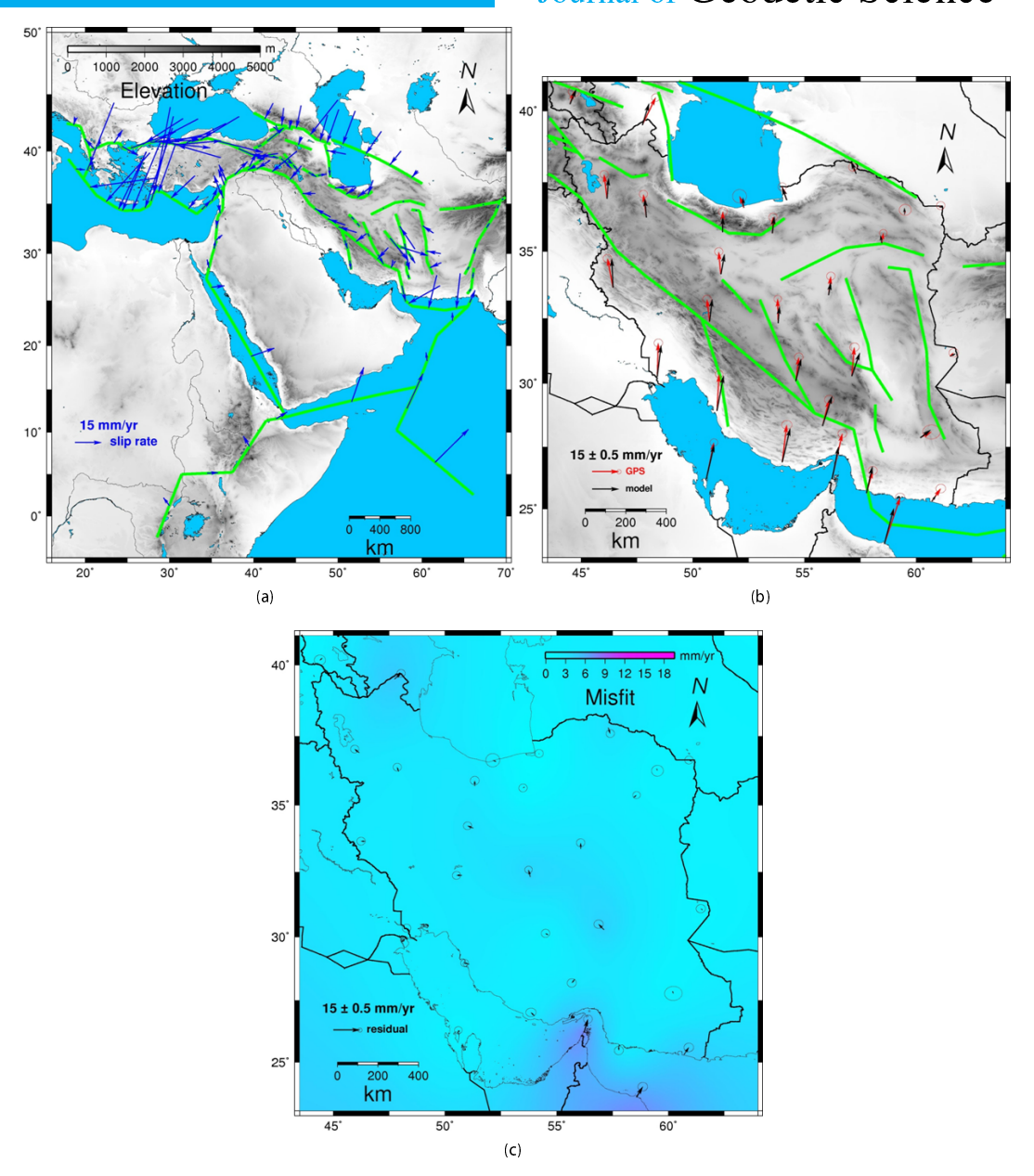


Figure 5. An optimal model. (a)The condition that no changes can be made to the regional model is now relaxed and some other local faults added. (b) Inside faults of Iran increase their velocity field amplitude and rotate it from SW-NE to N-S and SSE-NNW direction. (c) Most of the residuals are now below the errors quoted for the GPS velocity vectors. The interpretation presented in this Figure may change as more geologic and geodetic data are collected.

effects of strain accumulation. The distance of most of the GPS measurement points to the elements is significantly greater than locking depth. As a result, the contribution of interseismic strain is generally minor and the locking depth value has little effect in the modeling.

On the other hand sensitivity analysis was done to determine the sensitivity of the Okada (1985) model with respect to input

parameters. Our analysis shows that the model has maximum sensitivity to fault slip rate parameter and minimum sensitivity to the length of fault. Also this model has no sensitivity to lame coefficients in the Poisson solid case. It's important to note that this model sensitivity to slip rate of a fault is more than of sensitivity to fault locking depth. In GPS velocity field modeling, an average locking depth value (15 km) used for faults. Trial and error approach was done more on fault slip rate than locking depth.



Our model differs from rigid block models (Reilinger et al., 2006). While the GPS vectors can be fitted, dislocation conditions at the block boundaries are often incompatible with geological evidence. In our alternative strategy for modeling, it is assumed that faults are the surface expression of deeper structures. They consist of rectangular elements that extend from a locking depth of 15 km to 100,000 km (effectively infinite depth) in an elastic half space (Poisson's ratio 0.25). This simulates vertical structures that extend through the lower crust and upper mantle to the asthenosphere which are then modeled by dislocation elements in a half-space; a common approach to modeling GPS data (Savage and Burford, 1973). The slip vectors that fit the GPS velocity field are found by forward modeling.

In this approach slip is everywhere required to have a direction of motion consistent with geological constraints (focal mechanisms). The dislocations do not divide the region into closed rigid blocks and slip can vary along strike or die out as observed geologically. As a consequence, the lithosphere experiences elastic or plastic strain between the main structures for our models (Armijo et al., 2004; Flerit et al., 2003).

At the end we obtain a tectonic model for Arabia-Eurasia oblique collision zone with more details in NW Iran that is more realistic than the rigid block model (Reilinger et al., 2006) or models based on seismic or geologic strain rates only (Haines, 1982; Haines and Holt, 1993; Jackson et al., 1995; Masson et al., 2005) since (1) The modeling of present-day velocity field determined with GPS data incorporates geological constraints on the geometry of the main structures and on the long-term deformation; (2) The regions between major faults are not rigid and so the modeling allows for internal deformation.

4. GPS observations and modeling

Velocity measurements by GPS provide a direct image of the current velocities throughout the oblique collision zone of Arabian and Eurasian plates. The GPS observations on which this study is based are from campaign and continuous GPS networks in the region of Iran and eastern Turkey and are shown in Figure 2 (Eurasia fixed).

4.1. GPS observations

The GPS network used for modeling extends throughout Iran and from the Caspian Sea to the Iran/Turkey border (Figures 3(a) and 3(b)). The average distance between the two sites is about 30 to 70 km in the NW Iran, about 20 km in the vicinity of the Tabriz fault and about 300 km elsewhere. All continuous GPS benchmarks are setup on geodetically designed pillars deeply rooted in stable ground. Most campaign sites are anchored in bedrock, have a screw and small mast, forced centering setup, and have been surveyed for 48 h at least 3 times from 2000 to 2008. All campaigns and continuous GPS sites were measured with Ashtech Z12 and

Trimble 4000SSI receivers equipped with choke-ring antennas. Not all the CGPS sites were installed at the same time, KKDY and BZGN recorded for 1.6 yr, BZGN, ZARI, GGSH, KHJE, KLBR, HSTD, KRMD have more than 2 yr, but less than 2.5 yr of recording, MMKN, VLDN, YKKZ, BRMN, ARDH recorded data for 2.5 to 3 yr and POLD, TASJ, NZSF, BSOF, AMND, TABZ, SKOH, MNDB, AHAR, TKCE and RSHT have at least 3 yr of continuous recording.

The GAMIT/GLOBK software package (Herring et al., 2009a, b) was used to compute the coordinates and velocities of the sites using a three-step strategy (Dong et al., 1998; Feigl et al., 1993). GPS data of 14 IGS stations were introduced in the process to tie local network to the ITRF reference frame. Finally, velocities and their 1σ confidence uncertainties were estimated in ITRF 2005 and then the Eurasian reference frame was defined by minimizing the horizontal velocities of 23 IGS stations located in Europe and Central Asia (ARTU, BOR1, BRUS, GRAS, GRAZ, IRKT, JOZE, KOSG, KSTU, MADR, METS, NYAL, ONSA, POTS, TIXI, TOUL, TROM, VILL, WTZR, YAKT, ZECK, ZIMM, ZWEN). The WRMS value for the velocity residuals of these 23 sites is 0.1 mm/yr. There is good agreement between the SGPS and CGPS velocities for nearby Iranian sites since the differences are lower than 1 mm/yr. The GPS velocities and their uncertainties are given in Table 1 in a Eurasia-fixed reference frame. Then local velocity field combined with the velocity field of Reilinger et al. (2006) using the Euler Pole of rotation between common sites of two velocity fields (Hefty, 2007). Only 3 sites are common to the two solutions, the CGPS NSSP in Armenia and 2 SGPS sites in NW Iran (MIAN and BIJA). The RMS of the difference between local velocity solution and the Reilinger et al. (2006) solution is 0.69 mm/yr, within the average 2σ velocity uncertainty. Therefore we assume that there is no significant difference between the reference frames of these 2 velocity solutions. We used the combined velocity field for large-scale and detailed modeling.

4.2. Fault kinematic data

Fault elements of model were divided into two parts: (1) Inter-plate elements between Arabia, Eurasia, Africa and India tectonic plates and around Anatolian plateau. (2) Intra-plate elements within Iran with more details in the NW. Inter-plate elements location selected based on Reilinger et al. (2006) data. These elements used for large-scale modeling and are shown in Figure 4(a). By considering a schematic summary map showing the details of present day tectonic setting and kinematics of Iran in the Arabia and Eurasia convergence region (Figure 4(b)) intra-plate elements selected from Hessami and Jamali (2006). Figure 4(c) shows the selected known active faults of Iranian plateau as input dislocation elements for detailed modeling.



Table 1. East and north GPS velocity components (Ve, Vn) and 1σ uncertainties (σ_e , σ_n) in a Eurasia-fixed reference frame as determined by Djamour et al. (2011) and Reilinger et al. (2006). Latitude (lat.) and Longitude (long.) are given in degrees north and east, respectively. East (Ve) and North (Vn) velocity components and their uncertainties (σ_e and σ_n) are given in mm/yr. Corr. = correlation coefficient between the east and north uncertainties. An "*" in the site column designates continuous GPS stations. References are dj, (Djamour et al., 2011) and re, (Reilinger et al., 2006). Res. E and Res. N indicate misfit of each GPS site (residual velocities) from our best fit model.

Site	long. (° E)	lat. (°N)	Ve (mm/yr)	Vn (mm/yr)	σ _e (mm/yr)	$\sigma_{\rm n}$ (mm/yr)	Corr.	Ref.	Res. E (mm/yr)	Res. N (mm/yr)
AGKA	48.005	37.169	-0.57	12.39	0.58	0.59	0.005	di	-2.18	-0.25
AHAR*	47.050	38.468	1.93	9.13	0.18	0.25	-0.006	-	-1.25	-2.79
ALIS	51.082	28.919	1.24	21.61	0.81	0.75	0.001	re	-0.81	-0.37
AMAS	43.768	40.972	1.39	6.62	0.92	0.84	0.014	re	-0.43	024
AMND*	46.155	38.231	1.57	10.95	0.25	0.18	-0.007	di	0.09	0.30
ARBI	48.231	38.477	4.53	11.65	0.40	0.40	0.000	di	1.01	-0.81
ARDA	42.755	41.126	1.38	4.64	1.35	1.06	-0.012	di	-0.49	-2.60
ARDH*	47.650	37.829	1.23	11.88	0.26	0.40	-0.004	dj	-1.43	0.00
ARGI	43.026	39.719	0.84	8.66	0.68	0.65	-0.036	re	-0.12	-0.56
ARTI	43.954	40.609	1.99	8.18	0.83	0.82	-0.017	re	0.29	0.14
BAHR	50.608	26.209	4.33	21.93	0.47	-0.47	0.001	re	0.11	0.00
BALA	44.750	37.534	-3.38	15.00	0.59	0.60	0.010	dj	-2.39	1.42
BIJA	47.930	36.232	-1.98	13.10	0.39	0.39	0.001	re	-0.01	-2.89
BRMN*	47.288	37.919	1.59	12.40	0.38	0.21	-0.004	dj	-0.79	1.15
BSOF*	45.732	38.674	4.07	10.31	0.37	0.22	-0.004	dj	1.40	0.20
BZGN*	44.392	39.379	4.40	9.34	0.63	0.63	-0.001	dj	0.94	-0.46
DAMO	47.744	39.513	7.15	13.75	0.35	0.34	-0.003	dj	0.30	-1.62
GAGA	44.859	40.526	1.39	5.42	1.12	0.84	-0.007	re	-1.27	-2.88
GARN	44.742	40.149	2.86	9.76	0.62	0.54	0.006	re	0.50	0.29
GGSH*	44.954	38.207	2.80	13.15	0.69	0.70	-0.002	dj	3.26	0.65
GHO1	49.810	36.699	-1.25	12.29	0.73	0.76	-0.002	dj	-1.05	1.22
GHOT	44.428	38.489	-1.69	11.74	0.59	0.60	-0.040	dj	-0.92	-1.75
GOSM	48.419	38.706	5.07	12.24	0.91	0.80	0.003	re	1.40	-1.55
HARA	54.608	30.079	0.73	13.53	0.45	0.42	-0.001	re	0.29	-4.27
HEFZ	48.458	38.000	4.06	11.44	0.78	0.83	-0.017	dj	1.03	-1.27
HSTD*	47.094	37.576	-1.10	13.00	0.69	0.69	-0.001	dj	-1.38	1.69
JAM1	45.049	39.297	5.04	9.64	0.57	0.58	0.003	dj	1.20	-1.24
JERM	45.661	39.837	5.02	10.48	0.86	0.81	-0.015	re	0.17	-0.12
JOLF	45.605	38.952	4.01	10.52	0.60	0.61	0.008	dj	1.00	0.12
KAL2	43.341	38.549	-5.05	13.13	0.86	0.84	0.014	re	-2.70	0.52
KARS	43.170	40.685	1.54	5.92	0.59	0.50	-0.015	re	-0.08	-1.58
KASH	58.464	35.293	0.74	6.28	0.81	-0.75	0.001	re	0.04	1.02
KBLG*	44.565	39.031	3.41	11.90	0.79	0.80	-0.002	dj	0.10	1.18
KERM	57.119	30.277	0.47	15.88	0.56	0.48	0.000	re	-0.29	-0.66
KHAV	46.265	38.736	5.56	9.10	0.60	0.61	0.010	dj	2.34	-2.03
KHJE*	46.596	38.152	2.60	9.96	0.71	0.72	-0.001	dj	0.28	-0.46
KHOR	47.123	37.368	-2.63	12.87	0.60	0.61	0.009	dj	-3.10	1.40
KHOS	48.409	30.246	-0.49	18.22	1.23	1.09	0.003	re	0.96	2.36
KKDY*	44.160	39.332	5.30	9.34	0.83	0.83	-0.001	dj	2.32	-0.26
KLBR*	47.032	38.869	4.70	11.89	0.69	0.69	-0.001	dj	0.67	-0.47



Site	long. (°E)	lat.	Ve	Vn	$\sigma_{\rm e}$	$\sigma_{\rm n}$	Corr.	Ref.	Res. E	Res. N
] , ,	(° N)	(mm/yr)	(mm/yr)	(mm/yr)	(mm/yr)			(mm/yr)	(mm/yr)
KORD	54.199	36.860	-0.97	5.40	1.36	1.13	0.016	re	0.40	1.30
KRKT	41.794	38.754	-4.69	14.76	0.84	0.69	0.107	re	-1.27	2.84
KRYZ	42.149	39.714	-1.42	8.81	1.40	1.24	-0.022	re	-1.64	-0.66
LAMB	54.004	26.883	2.91	22.54	1.63	1.17	0.012	re	-3.32	3.36
МАНМ	52.285	36.588	-1.93	6.21	1.13	1.10	0.007	re	3.55	-4.80
MARG	48.890	37.187	-0.04	10.92	0.74	0.77	-0.010	dj	-1.27	-2.25
MIAN	46.162	36.908	-2.16	13.54	0.41	0.39	0.000	re	0.56	-2.70
MM KN*	44.771	37.985	-1.52	9.88	2.43	0.97	0.000	dj	-0.62	-3.37
MMOR	44.114	40.178	2.43	7.87	0.83	0.82	-0.017	re	0.76	-0.45
MOGH	48.049	39.013	5.71	10.64	0.77	0.81	-0.012	dj	0.72	-3.74
MUSC	58.569	23.564	6.60	26.64	1.24	1.07	0.001	re	-1.62	-2.55
NORA	46.093	39.536	4.20	10.11	0.99	0.88	0.026	re	-0.94	-1.32
NSSP*	44.503	40.226	2.16	7.17	0.13	0.12	-0.013	dj	0.48	-1.78
NZSF*	45.114	38.999	3.93	8.22	0.69	0.69	-0.001	dj	0.68	-2.45
OLTU	41.990	40.548	1.95	5.07	0.93	0.90	0.020	re	0.82	-2.75
ORTA	47.869	37.929	3.49	13.08	0.57	0.58	0.005	dj	0.54	0.83
PIRM	47.157	38.984	4.74	11.46	0.59	0.60	0.005	dj	0.26	-1.18
POLD*	45.062	39.351	4.31	9.61	0.20	0.22	-0.007	dj	0.43	-1.29
PTNS	42.910	39.232	-2.03	9.45	0.61	0.52	-0.032	re	-0.01	-1.42
RESD	42.547	38.488	-5.62	14.01	1.52	1.20	-0.045	re	-2.53	1.80
ROBA	56.070	33.369	1.87	11.23	1.26	1.09	0.006	re	2.12	1.56
SEMN	53.564	35.662	-0.01	9.17	1.32	1.13	0.014	re	-0.14	-2.00
SHAB	45.887	38.228	1.60	11.98	0.41	0.41	0.004	dj	0.97	1.15
SHAH	50.748	32.367	-2.26	12.70	0.44	0.42	-0.004	re	0.74	-3.52
SHIR	57.308	37.814	2.28	2.58	1.38	1.11	0.020	re	-0.06	-1.82
SKOH	46.123	37.933	-0.07	12.85	0.28	0.56	-0.002	dj	0.65	2.06
SOLH	41.057	38.959	-6.75	11.47	1.43	1.20	-0.024	re	-2.29	-1.85
TABZ*	46.343	38.056	0.22	12.76	0.26	0.43	-0.002	dj	0.09	2.09
TASJ*	45.361	38.316	-0.27	12.81	0.20	0.33	-0.006	dj	-0.83	1.80
TAZA	47.271	38.270	3.32	11.38	0.54	0.56	0.004	dj	0.18	-0.46
TEHN	51.334	35.697	0.22	12.66	0.70	0.69	0.000	re	1.30	1.00
VARZ	46.603	38.178	2.49	11.73	0.46	0.46	-0.004	dj	0.02	1.26
VLDN*	45.193	38.492	2.87	13.79	0.26	0.29	-0.004	dj	1.65	2.72
YARD	48.388	38.952	5.30	13.03	0.93	0.85	0.002	re	0.57	-1.76
YKKZ*	45.414	38.672	4.17	9.90	0.51	0.36	-0.003	dj	1.86	-0.65
YAZT	61.034	36.601	-3.54	0.01	1.29	1.11	0.010	re	-0.38	0.28
ZABO	61.517	31.049	1.20	0.15	1.20	1.06	0.004	re	-1.22	-1.07
ZARI*	44.550	38.446	0.19	12.27	0.64	0.64	-0.001	dj	0.85	-1.02

4.3. Large-scale modeling in the Middle-East and detailed modeling in Iran

Deformation is calculated using the results for rectangular dislocation elements of Okada (1985) in a similar manner to that described by Armijo et al. (2004), Flerit et al. (2003) and Jackson and McKenzie (1988). Model velocity field are then compared with GPS velocity field. The vectors are consistent with geological rates and produce an overall velocity field consistent with the larger scale

plate motions (determined from the pole of rotation).

According to Figure 10 and Table 2 of Appendix A, relative plate motions between Arabian, Nubia, Somalian, Indian plates and around Anatolian plateau included in the model with slip direction and amplitudes (in blue) predicted by, the plate motion without any dislocation in Iran. The motions on these certain boundaries are known and are not free parameters in the modeling. They are fixed in both amplitude and direction (Reilinger et al., 2006) (Figure 5(a)) In Figure 5(b) the initial large-scale model is shown allowing the



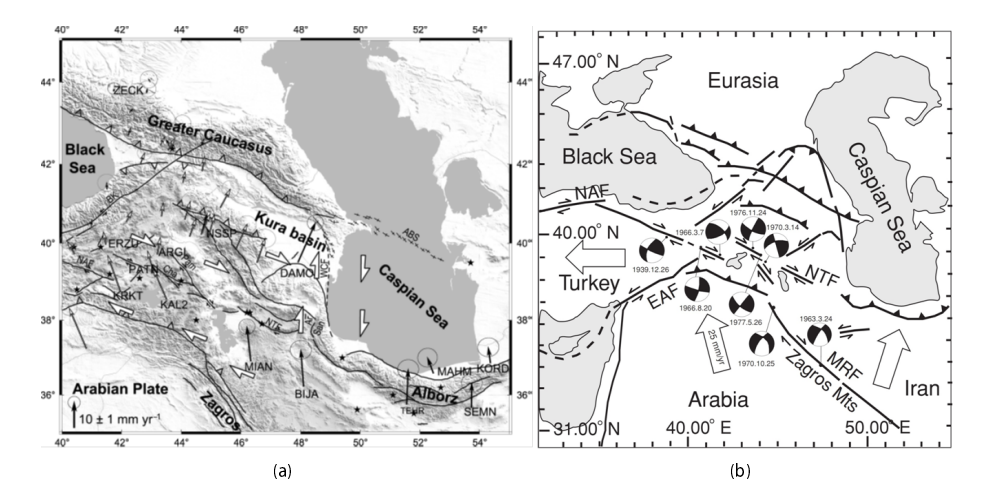


Figure 6. Geological and seismological constraints used for detailed modeling in the NW Iran. (a) GPS horizontal velocities and their 95% confidence ellipses (in the Eurasia-fixed reference frame) for the NW Iran, eastern Turkey and Caucasus area. Black vectors are from Vernant (2004b) and black with white heads from the McClusky et al. (2000). The velocities for the NSSP station are quite similar. Right stepping en echelon fold axis are plotted near the WCF. ABS: Apsheron Balkan Sills, Ar: Ardebil Fault, BK: Borzhomi-Kazbeg, Cha: Chalderan, NAF: North Anatolian Fault, NTF: North Tabriz Fault, Pam: Pambuk, San: Sangavar Fault, WCF: West Caspian Fault. Historical seismicity (M > 7) from the NEIC catalogue is indicated by black stars. After Vernant et al. (2004b) (b) Location map of the NW Iran-Eastern Turkey, with focal mechanisms of some of the large earthquakes (mb > 5.3) in the Tabriz-Chaldiran seismogenic zone. North Tabriz Fault (NTF), East Anatolian Fault (EAF), Main Recent Fault (MRF), North Anatolian Fault (NAF). After Hessami et al. (2003).

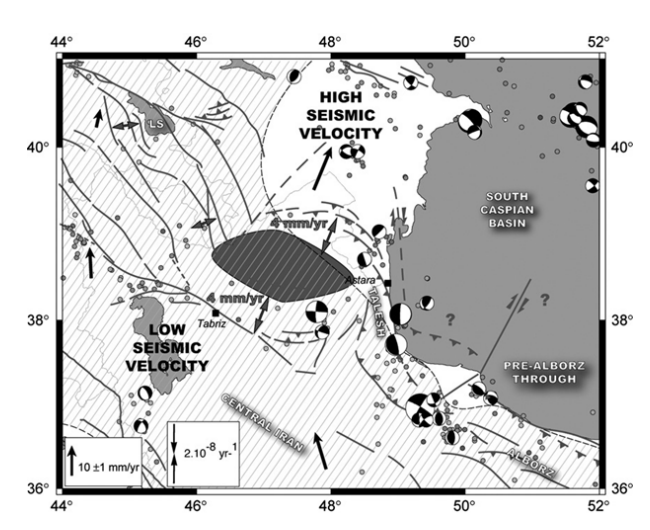


Figure 7. Synthetic sketch summarizing the main results of Masson et al. (2006): right-lateral movement along the Tabriz fault, extension north of the Tabriz fault, subduction of the South Caspian and Kura basins, uncoupling of the Talesh and the Alborz. Shaded area indicates the Talesh block. After Masson et al. (2006).

Eurasia fixed GPS velocity vectors and the model vectors to be compared. Large-scale model elements create a velocity field in the SW-NE direction with amplitudes decreasing in the mentioned direction. Figure 5(c) shows residuals plus shading indicating the degree of misfit. It's calculated by interpolating between scalar

values of the misfit. Continuous curvature splines in tension used for interpolation (Smith and Wessel, 1990). It makes easy to see where misfits are greatest. This is a reliable method for identifying systematic errors in groups of vectors and hence for systematically improving a model. A global rms misfit represented by a single number gives little guide to how a model can be improved. Large residuals are visible southwest of Iran parallel and perpendicular to oblique collision zone of Arabia and Eurasia plates (Figure 5(c)).

Then intra-plate elements within Iran included in the model progressively (Figure 4(c)). For these elements, geological and seismological data (fault traces and direction of motion shown by focal mechanisms) used to constrain the slip rate vectors direction, with the amplitudes being determined to fit the observed velocity vectors. The procedure for arriving at a final model for the velocity field is by trial and error in slip rates direction and amplitude. Provided that the elements geometry selected from the geology is correct the solution is unique within the limits of data error. The geological and seismological data included in our model provide major constraints not adopted in other approaches. Figure 6(a) shows all of these elements with slip rates (in blue). It shows a satisfactory model. The details of this model are poorly constrained however, and it may not be fully supported in the future as errors in the velocity vectors are progressively reduced as more GPS data accumulates. Figure 6(b) allows the GPS velocity vectors (in red) and the detail modeling velocity vectors (in black) associated with all of model elements to be compared after trial and error approach in boundary conditions. Figure 6(c) shows the resultant reduced residuals plus shading indicating the degree of misfit. With few

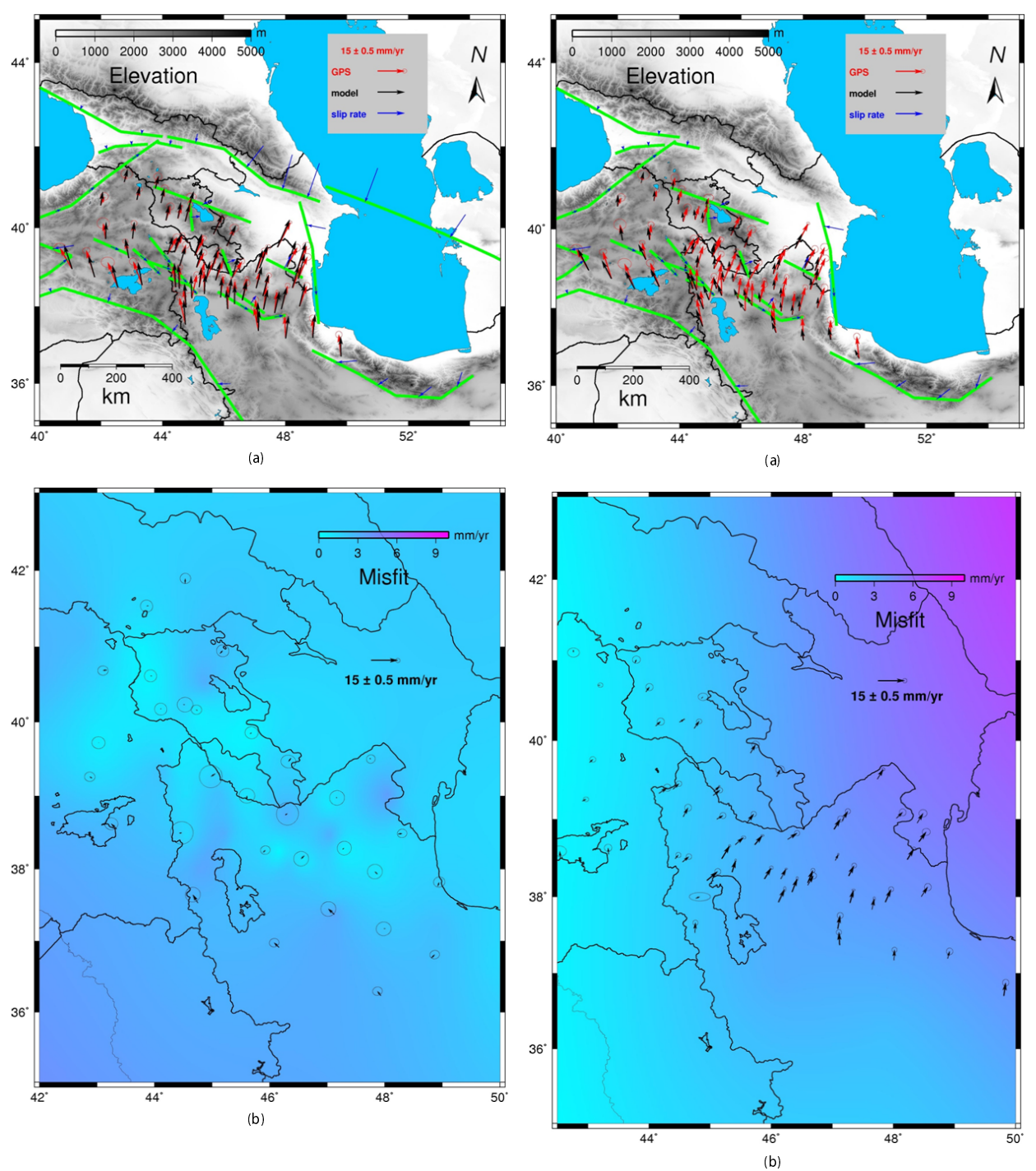


Figure 8. GPS velocity vectors modeling in the NW Iran. Motion is referenced to fixed Eurasia. (a) Comparison of the modeled vectors (in black) with the observed vectors (in red). The ellipses are at 95% confidence limits from Djamour et al. (2011). Blue vectors show best fit model slip rates. (b) Residual vectors (in black) plus shading (in red) indicating the degree of misfit.

Figure 9. Same as Figure 8 without subduction motion of the South Caspian and Kura basins. (a) Model vectors have low amplitude in comparison with observed vectors. (b) Residual vectors and shading indicating a systematic effect in the model without mentioned subductions.



exceptions the fit is within the quoted error ellipses of Reilinger et al. (2006). The remaining misfits are not systematically distributed indicating that individual sites are anomalous or are affected by small local structures.

Comparing Figure 4 and Figure 5 indicate that inside faults of Iran increase their velocity field amplitude and rotate it from SW-NE to N-S and SSE-NNW direction.

5. Detailed modeling for NW Iran

To continue more detailed modeling in NW Iran, dense GPS velocity vectors selected from Djamour et al. (2011) (Table 1). Figure 3(b) shows GPS data used for this purpose with their 95% confidence limits for this region. Motion is referenced to fixed Eurasia. Then active faults in this region selected with more details according to Vernant et al. (2004b) (Figure 7(a)) and Hessami et al. (2003) (Figure 7(b)).

Modeling results using just strike slip and thrust faults as expected by Arabia-Eurasia collision are not consistent with GPS data in this region. On the other hand according to Masson et al. (2006) GPS data indicates four extensional regions. Extensional regions show locations for four possible normal faults in this region (Figure 7). We considered four normal faults in these regions and then began to modeling by trial and error approach to get a good fit between GPS and model velocity fields for NW Iran. The root mean square of best fitting model in the NW Iran calculated as 0.26 mm. It shows that there is a good consistency between our modeling results and GPS data.

Figure 9(a) allows that the best fitting model vectors (in black) to be compared with observed GPS vectors (in red). It also shows the elements (in green) with model slip rates (in blue) on them used for modeling in different parts of the fault system within this region. The model includes the larger scale structures shown in Figures 7(a) and 7(b). This adds motion consistent with structures beneath some mapped minor faults. Figure 9(b) shows the residual vectors (in black) plus shaded error field (in red) indicating the degree of misfit. As it can be seen in Figure 9(b) most of residuals are within 95% confidence limit of GPS velocity vectors. This statistical equivalence between GPS and model velocity vectors is an indication of satisfactory tectonic modeling in NW Iran. Using dislocation theory slip rate values were estimated between 2 ~ 5 mm/yr for normal faults shown in Figure 9(a). The details of elements used for large-scale and detailed modelling provided in Appendix A (Figure 10; Table 2). Columns 10 and 11 of Table 1 show the misfit of each GPS site (residual velocities) from our best fit model.

Then we removed the South Caspian and Kura basin subduction elements from the best fit model. In this case model vectors have low amplitude in comparison with observed vectors (Figure 10(a)). Residual vectors and shading indicate a systematic effect in the model without mentioned subductions (Figure 10(b)). Comparing Figures 8 and 9 indicates that the deformation in the NW Iran is

influenced both by Arabia-Eurasia collision and subduction motion of the South Caspian and Kura basins basement beneath the Apsheron-Balkhan sill and the Great Caucasus respectively. Such that these subductions increase the model velocity magnitudes and rotate it from NNW to NNE direction. We suggest that the normal faulting in NW Iran could be due to these subductions. So our model proves the idea that the existence of these subductions explains the extension observed by GPS vectors in the core of the Arabia-Eurasia collision.

6. Conclusions

The concepts of dislocation theory can be applied to the deformation modeling of different parts of Middle East. We have first produced an overall model of the regional displacement field for Iran, consistent with the large-scale kinematics of Arabia and Eurasia collision and with geological features known to be active. In general, this correctly describes the displacement field in Iran, but closer to it the fit to the data is poor. To fit observations better, more detailed slip partitioning among faults is required. The resultant tectonic model is more realistic than the rigid block model or velocity field obtained by seismicity.

Modeling results show that the existence of the South Caspian and Kura basins subduction are essential to explain the extension observed by GPS and provide a good agreement between GPS and model velocity fields.

Our model proves the existence of subduction of the South Caspian and Kura basins in the core of the Arabia-Eurasia collision. It explains the extension observed by GPS in the core of the Arabia-Eurasia collision. It shows that this region is not only affected by Arabia-Eurasia collision but also contributes in the subduction motion of the South Caspian and Kura basins basement beneath the Apsheron-Balkhan sill and the Great Caucasus respectively. For observed extension we estimated slip rates for four probable normal faults in the extensional regions between 2 ~ 5 mm/yr. To get better results for slip partitioning, using more dense GPS networks in the study region is highly recommended.

Partitioned slip rates using dislocation theory could be used to improve seismic hazard analysis in the study area.

Appendix A

The Arabia-Eurasia motion fits the motion defined by Djamour et al. (2011) and Reilinger et al. (2006). Slip rates for elements in Iran have direction compatible with geological and seismological constraints. Their magnitude is adjusted for the model to fit the GPS velocity vectors.

Table 2 provides the latitude and longitude of elements and slip rate values used to calculate the vector field shown in Figures 3(a) and 3(b) of the main text. Figure 10 shows the location of the elements in map form.



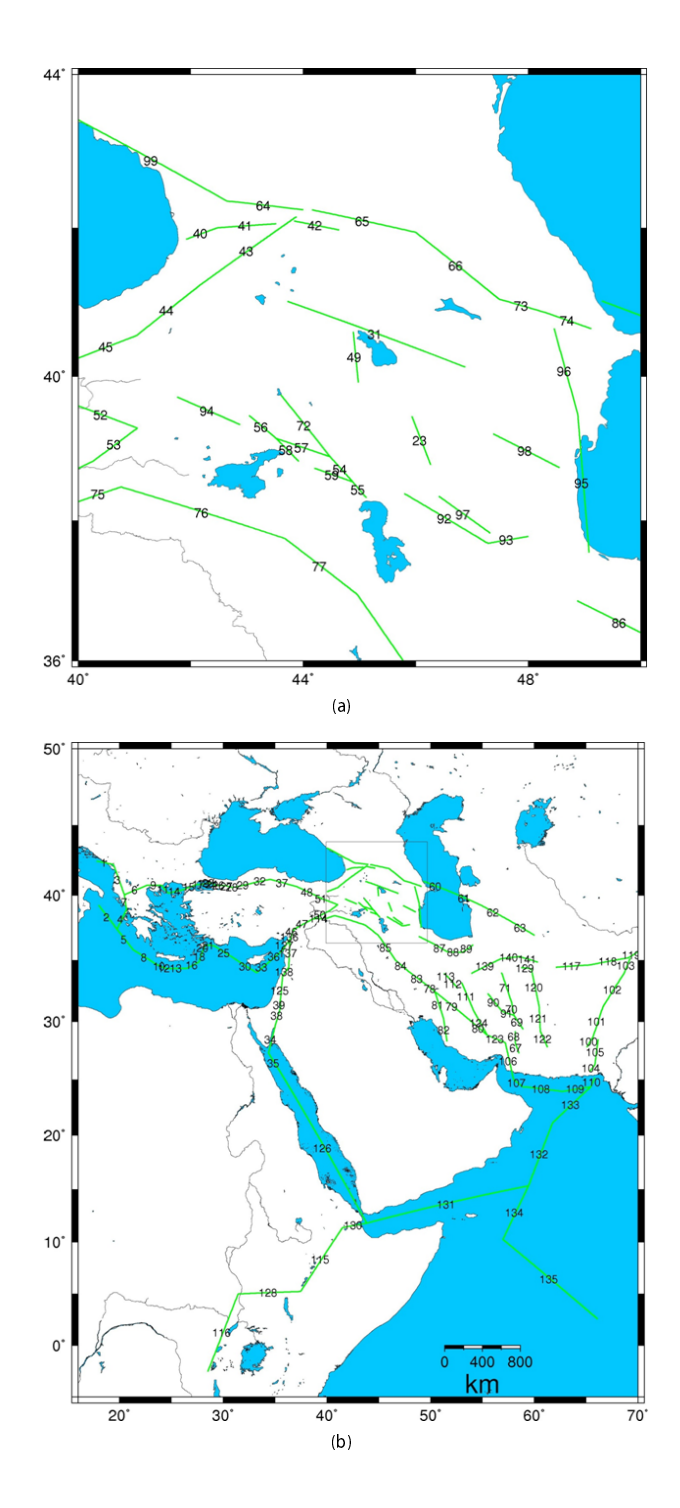


Figure 10. Map of elements. (a) The elements visible in Figure 9(a) in the main text are shown. The numbers identify the corresponding elements in Table 2. (b) Elements of the model over a larger region than that where GPS velocity vectors are modelled in detail. The numbers identify the corresponding elements in Table 2.



Table 2. Location (longitude and latitude) of elements and slip rate values. References are re, (Reilinger et al., 2006); ts (this study). Elements of Reilinger et al. (2006) used for large-scale modeling. Total slip rates are those shown in Figure 4a. Elements of this study used for detailed modeling with more details in the NW Iran. Total slip rates are those shown in Figures 5a and 8a. Left-lateral slip and closing of an element is positive. Locking depth indicates the depth to the base of the locked zone.

Element number	Element start long. (°E) lat.(°N)		Element end			Total slip rate (mm/year) Left lateral Closing		REF.
			long. (°E)					
1	17.79	42.48	19.42	42.23	15.0	0.3	3.8	re
2	17.98	39.26	19.76	37.42	15.0	-3.6	-3.8	re
3	19.42	42.23	20.47	40.02	15.0	-7.3	3.0	re
4	19.76	37.42	20.68	38.92	15.0	-41.3	2.7	re
5	19.76	37.42	21.32	35.81	15.0	-19.8	33.3	re
6	20.47	40.02	22.72	40.74	15.0	2.4	-3.8	re
7	20.47	40.02	20.68	38.92	15.0	-7.6	0.5	re
8	21.32	35.81	23.65	34.62	15.0	-6.7	36.5	re
9	22.72	40.74	24.04	40.73	15.0	4.8	-7.2	re
10	23.65	34.62	24.27	34.39	15.0	-1.4	35.9	re
11	24.04	40.73	24.70	40.14	15.0	9.8	-3.6	re
12	24.27	34.39	24.61	34.34	15.0	6.2	35.1	re
13	24.61	34.34	26.53	34.36	15.0	17.1	38.8	re
14	24.70	40.14	26.17	40.41	15.0	-26.8	-2.8	re
15	26.17	40.41	27.49	40.80	15.0	-26.5	5.4	re
16	26.53	34.36	27.65	34.84	15.0	34.7	32.8	re
17	27.49	40.80	28.00	40.80	15.0	-27.5	-0.9	re
18	27.65	34.84	28.01	35.71	15.0	49.5	3.3	re
19	28.00	40.80	28.50	40.89	12.0	-26.9	6.8	re
20	28.01	35.71	28.27	36.22	15.0	49.0	10.6	re
21	28.27	36.22	29.14	36.13	15.0	6.1	27.5	re
22	28.50	40.89	28.88	40.89	12.0	-27.9	2.3	re
23	45.93	39.45	46.27	38.78	15.0	0.0	-2.0	ts
24	28.88	40.89	29.24	40.71	12.0	-24.6	-12.7	re
25	29.14	36.13	31.27	35.02	15.0	-4.7	17.8	re
26	29.24	40.71	30.14	40.72	15.0	-27.1	5.8	re
27	30.14	40.72	30.77	40.58	15.0	-28.0	0.1	re
28	30.77	40.58	31.20	40.60	15.0	-24.6	-0.6	re
29	31.20	40.60	32.85	40.89	15.0	-24.2	5.5	re
30	31.27	35.02	33.22	33.99	15.0	1.0	9.3	re
31	43.72	41.02	46.88	40.12	15.0	-4.0	4.0	ts
32	32.85	40.89	34.51	41.16	15.0	-24.2	8.0	re
33	33.22	33.99	34.45	34.88	15.0	7.0	-0.5	re
34	34.37	27.29	35.01	29.61	15.0	4.5	-2.2	re
35	34.37	27.29	35.57	25.55	15.0	3.2	-6.8	re
36	34.45	34.88	35.62	35.69	15.0	7.0	-3.5	re
37	34.51	41.16	37.13	40.62	15.0	-25.8	-0.2	re
38	35.01	29.61	35.58	31.32	15.0	4.5	-0.6	re
39	35.47	31.38	35.58	31.32	15.0	1.3	-4.3	re
40	41.92	41.85	42.48	42.00	15.0	0.0	2.0	ts



Element	Element		Element		Locking depth	Total slip rat	REF.	
number	start	start		end				
	long. (°E) la	nt.(°N)	long. (°E) la	t.(°N)	(km)	Left lateral (Closing	
41	42.48	42.00	43.52	42.05	15.0	0.0	2.0	ts
42	43.84	42.09	44.64	41.97	15.0	0.0	3.0	ts
43	42.16	41.23	43.88	42.15	15.0	5.0	0.0	ts
44	41.04	40.55	42.16	41.23	15.0	4.0	0.0	ts
45	40.00	40.25	41.04	40.55	15.0	3.0	0.0	ts
46	36.63	37.03	36.83	37.42	15.0	6.8	-7.1	re
47	36.83	37.42	38.65	38.20	15.0	9.9	-2.9	re
48	37.13	40.62	39.33	39.81	15.0	-15.7	-0.4	re
49	44.89	40.60	44.98	39.91	15.0	0.0	-3.0	ts
50	38.65	38.20	40.27	38.83	15.0	7.0	-5.1	re
51	39.33	39.81	39.80	39.65	15.0	-15.6	4.5	re
52	39.80	39.65	41.05	39.29	15.0	-10.3	5.8	re
53	40.27	38.83	41.05	39.29	15.0	5.0	-0.2	re
54	44.48	38.89	44.88	38.54	15.0	-3.0	0.0	ts
55	44.88	38.54	45.12	38.32	15.0	-3.0	0.0	ts
56	43.04	39.46	43.52	39.14	15.0	-5.0	0.0	ts
57	43.52	39.14	44.48	38.89	15.0	-5.0	0.0	ts
58	43.52	39.14	43.92	38.83	15.0	-5.0	0.0	ts
59	44.20	38.73	44.88	38.54	15.0	0.0	0.0	ts
60	49.31	41.02	51.89	40.26	15.0	0.0	20.0	ts
61	51.89	40.26	54.82	39.26	15.0	-3.0	15.0	ts
62	54.82	39.26	57.51	38.13	15.0	-2.0	10.0	
63	57.51	38.13	60.02	36.95	15.0	-1.0	5.0	ts
64	42.64	42.35	44.00	42.24	15.0	0.0	2.0	ts re
65	44.16	42.33	46.00	41.94	15.0	0.0	5.0	re
66	46.00	41.94	47.48	41.05	15.0	0.0	15.0	re
67	58.17	28.20	58.51	27.28	15.0	-1.0	0.0	
-		+		29.18	15.0	0.0	0.0	ts
68	58.17 58.04	28.20	58.17	29.18	15.0	-6.0		ts
70		30.50	58.92 58.04		15.0		0.0	ts
-	57.83	31.52		30.50		-15.0	0.0	ts .
71	56.85	34.00	57.83	31.52	15.0	-15.0	4.0	ts
72	43.60	39.75	44.48	38.89	15.0	-6.0	0.0	ts
73	47.48	41.05	48.32	40.86	15.0	0.0	20.0	re
74	48.32	40.86	49.12	40.65	15.0	0.0	20.0	re
75	40.00	38.26	40.76	38.47	15.0	0.0	2.0	ts
76	40.76	38.47	43.68	37.74	15.0	0.0	5.0	ts
77	43.68	37.74	44.96	36.95	15.0	0.0	5.0	ts
78	49.74	32.92	50.40	32.47	15.0	0.0	4.0	ts
79	50.40	32.47	53.95	29.97	15.0	0.0	7.0	ts .
80	53.95	29.97	55.45	28.83	15.0	0.0	9.0	ts .
81	50.40	32.47	51.25	30.21	15.0	-5.0	0.0	ts .
82	51.25	30.21	51.58	28.30	15.0	-5.0	0.0	ts .
83	47.90	34.08	49.74	32.92	15.0	0.0	3.0	ts
84	46.61	35.00	47.90	34.08	15.0	0.0	2.0	ts
85	44.96	36.95	46.61	35.00	15.0	-4.0	6.0	ts
86	48.87	36.86	50.42	36.23	15.0	10.0	6.0	ts
87	50.42	36.23	51.59	35.67	15.0	3.0	6.0	ts



Element number	Element start			Element end		Total slip rate (mm/year)		REF.	
	long. (°E) l	at.(°N)	long. (°E)	lat.(°N)		Left later	Left lateral Closing		
88	51.59	35.67	53.06	35.60	15.0	7.0	6.0	ts	
89	53.06	35.60	54.11	36.20	15.0	7.0	5.0	ts	
90	55.52	32.30	56.90	30.82	15.0	-16.0	0.0	ts	
91	56.90	30.82	58.04	30.50	15.0	-16.0	0.0	ts	
92	45.80	38.38	47.28	37.68	15.0	-5.0	0.0	ts	
93	47.28	37.68	48.00	37.77	15.0	-5.0	0.0	ts	
94	41.76	39.71	42.88	39.33	15.0	-5.0	0.0	ts	
95	49.08	37.55	48.88	39.48	15.0	-5.0	0.0	ts	
96	48.46	40.65	48.88	39.48	15.0	-5.0	10.0	ts	
97	46.41	38.34	47.33	37.82	15.0	0.0	-2.0	ts	
98	47.38	39.21	48.56	38.74	15.0	0.0	-5.0	ts	
99	40.00	43.41	42.64	42.35	15.0	0.0	2.0	ts	
100	65.08	27.80	65.69	28.73	15.0	1.0	0.0	ts	
101	65.69	28.73	66.62	31.20	15.0	2.0	0.0	ts	
102	66.62	31.20	68.69	34.00	15.0	1.0	0.0	ts	
103	68.69	34.00	69.23	35.13	15.0	1.0	0.0	ts	
104	65.38	25.71	65.85	26.27	15.0	1.0	0.0	ts	
105	65.85	26.27	66.15	28.47	15.0	2.0	0.0	ts	
106	57.20	28.19	58.00	25.00	15.0	8.0	0.0	ts	
107	58.00	25.00	58.85	24.36	15.0	5.0	19.0	ts	
108	58.85	24.36	62.69	23.93	15.0	0.0	19.0	ts	
109	62.69	23.93	65.46	24.36	15.0	0.0	19.0	ts	
110	65.46	24.36	65.85	25.14	15.0	5.0	0.0	ts	
111	53.00	33.20	54.14	30.89	15.0	-4.0	0.0	ts	
112	51.92	33.43	52.62	32.73	15.0	-2.0	0.0	ts	
113	51.31	33.95	51.92	33.43	15.0	-2.0	0.0	ts	
114	40.00	38.26	38.65	38.20	15.0	0.0	2.0	re	
115	37.47	5.235	41.51	11.38	15.0	3.0	-6.0	re	
116	28.52	-2.54	31.45	5.001	15.0	2.9	-4.7	re	
117	62.08	34.44	65.38	34.63	15.0	0.0	0.0	ts	
118	65.38	34.63	69.08	35.19	15.0	0.0	0.0	ts	
119	69.08	35.19	69.92	35.63	15.0	0.0	0.0	ts	
120	59.71	34.31	60.46	31.28	15.0	-5.2	5.0	ts	
121	60.46	31.28	60.58	29.18	15.0	-1.9	8.0	ts	
122	60.58	29.18	61.27	27.80	15.0	0.0	7.0	ts	
123	55.45	28.83	57.20	28.19	15.0	0.0	2.0	ts	
124	54.14	30.89	55.45	28.83	15.0	-6.0	0.0	ts	
125	35.47	31.38	35.72	33.68	12.0	4.4	0.1	re	
126	35.57	25.55	43.84	11.79	15.0	2.9	-13.5	re	
127	35.62	35.69	36.43	36.63	15.0	5.5	-7.9	re	
128	31.45	5.00	37.47	5.235	15.0	6.1	-0.1	re	
129	58.74	34.41	59.71	34.31	15.0	2.0	0.0	ts	
130	41.51	11.38	43.84	11.79	15.0	6.8	-2.6	re	
131	43.84	11.79	59.44	15.32	0.0	-11.6	-17.1	re	
132	59.44	15.32	61.77	21.12	15.0	-4.4	-2.3	re	
133	61.77	21.12	65.46	24.36	15.0	-3.2	-3.4	re	
134	59.44	15.32	56.98	10.23	15.0	21.6	-0.2	re	



Element number	Element start		end		Locking depth (km)	Total slip rate (mm/year)		REF.
	long. (°E) lat	g. (°E) lat.(°N) long. (°E) lat.(°N)]	Left lateral Closing			
135	56.98	10.23	66.12	2.54	15.0	2.6	-26.5	re
136	36.43	36.63	36.63	37.03	15.0	6.8	-6.4	re
137	36.31	34.44	36.430	36.63	15.0	4.8	2.0	re
138	35.72	33.68	36.31	34.44	15.0	3.5	3.1	re
139	53.94	33.94	56.80	35.12	15.0	0.0	0.0	ts
140	56.80	35.12	58.56	35.29	15.0	2.0	0.0	ts
141	58.56	35.29	60.35	34.84	15.0	0.0	0.0	ts

References

Alavi, M., 1994. Tectonics of the Zagros orogenic belt of Iran: new data and interpretations. Tectonophysics 229, 211-238. Allen, M.B., Ghassemi, M.R., Shahrabi, M., Qorashi, M., 2003. Accommodation of late Cenozoic oblique shortening in the Alborz range, northern Iran. Journal of Structural Geology 25, 659-672.

Ambraseys, N.N., Melville, C.P., 1982. A History of Persian Earthquakes. Cambridge University Press, New York.

Armijo, R., Flerit, F., King, G., Meyer, B., 2004. Linear elastic fracture mechanics explains the past and present evolution of the Aegean. Earth and Planetary Science Letters 217, 85-95.

Bachmanov, D.M., Trifonov, V.G., Hessami, K.T., Kozhurin, A.I., Ivanova, T.P., Rogozhin, E.A., Hademi, M.C., Jamali, F.H., 2004. Active faults in the Zagros and central Iran. Tectonophysics 380, 221-241.

Bayer, R., Chéry, J., Tatar, M., Vernant, P., Abbassi, M., Masson, F., Nilforoushan, F., Doerflinger, E., Regard, V., Bellier, O., 2006. Active deformation in Zagros-Makran transition zone inferred from GPS measurements. Geophysical Journal International 165, 373-381.

Berberian, F., Muir, I.D., Pankhurst, R.J., Berberian, M., 1982. Late Cretaceous and early Miocene Andean-type plutonic activity in northern Makran and Central Iran. J. Geol. Soc. 139, 605-614. Berberian, M., 1983. The southern Caspian: A compressional depressionfloored by a trapped, modified oceanic crust." Canadian Journal of Earth Sciences 20, 163-183.

Berberian, M., 1995. Master "blind" thrust faults hidden under the Zagros folds: active basement tectonics and surface morphotectonics. Tectonophysics 241, 193-195.

Berberian, M., Yeats, R.S., 2001. Contribution of archaeological data to studies of earthquake history in the Iranian Plateau. Journal of Structural Geology 23, 563-584.

Canitez, N., 1969. The focal mechanisms in Iran and their relations to tectonics. Pure and Applied Geophysics 75, 76-87. Chandra, U., 1984. Focal mechanism solutions for earthquakes in Iran. Physics of The Earth and Planetary Interiors 34, 9-16.

Copley, A., Jackson, J., 2006. Active tectonics of the Turkish-Iranian Plateau. Tectonics 25, TC6006.

Djamour, Y., Vernant, P., Bayer, R., Nankali, H.R., Ritz, J.-F., Hinderer, J., Hatam, Y., Luck, B., Le Moigne, N., Sedighi, M., Khorrami, F., 2010. GPS and gravity constraints on continental deformation in the Alborz mountain range, Iran. Geophysical Journal International 183, 1287-1301.

Djamour, Y., Vernant, P., Nankali, H.R., Tavakoli, F., 2011. NW Iran-eastern Turkey present-day kinematics: Results from the Iranian permanent GPS network. Earth and Planetary Science Letters 307, 27-34.

Dong, D., Herring, T.A., King, R.W., 1998. Estimating regional deformation from a combination of space and terrestrial geodetic data. Journal of Geodesy 72, 200-214.

Falcon, N.L., 1974. Southern Iran: Zagros Mountains, in Mesozoic-Cenozoic Orogenic Belts, Data for Orogenic Studies. Geological Society of London Special Publication, 199-211. Falcon, N.L., 1976. The Minab Anticline: the Geological Evolution of Southern Iran: the report of the Iranian Makran expedition. Geographical Journal 142, 409-410.

Feigl, K.L., Agnew, D.C., Bock, Y., Dong, D., Donnellan, A., Hager, B.H., Herring, T.A., Jackson, D.D., Jordan, T.H., King, R.W., Larsen, S., Larson, K.M., Murray, M.H., Shen, Z., Webb, F.H., 1993. Space Geodetic Measurement of Crustal Deformation in Central and Southern California, 1984-1992. J. Geophys. Res. 98, 21677-21712.

Flerit, F., Armijo, R., King, G.C.P., Meyer, B., Barka, A., 2003. Slip partitioning in the Sea of Marmara pull-apart determined from GPS velocity vectors. Geophysical Journal International 154, 1-7.

Hager, B.H., King, R.W., Murray, M.H., 1991. Measurement of Crustal Deformation Using the Global Positioning System. Annual Review of Earth and Planetary Sciences 19, 351-382.

Haines, A.J., 1982. Calculating velocity fields across plate boundaries from observed shear rates. Geophysical Journal of the Royal Astronomical Society

68, 203-209. Haines, A.J., Holt, W.E., 1993. A Procedure for Obtaining the Complete Horizontal Motions Within Zones of Distributed Deformation From the Inversion of Strain Rate Data. J. Geophys. Res. 98, 12057-12082.



Haynes, S.J., McQuillan, H., 1974. Evolution of the Zagros Suture Zone, Southern Iran. Geological Society of America Bulletin 85, 739-744

Hefty, J., 2007. Geo-kinematics of central and south-east Europe resulting from combination of various regional GPS velocity fields. Acta Geodynamica et Geomaterialia 4, 173-189.

Herring, T.A., King, R.W., McClusky, S.C., 2009a. GAMIT reference manual, Release 10.3. Massachussets Institute of Technology, Cambridge.

Herring, T.A., King, R.W., McClusky, S.C., 2009b. Introduction to GAMIT/GLOBK, Release 10.35. Massachussetts Institute of Technology, Cambridge.

Hessami, K., Jamali, F., 2006. Explanatory Notes to the Map of Major Active Faults of Iran. Journal of Seismology and Earthquake Engineering (JSEE) 8, 1-11.

Hessami, K., Koyi, H.A., Talbot, C.J., Tabassi, H., Shabanian, E., 2001. Progressive unconformities within an evolving foreland fold-thrust belt, Zagros mountains. J. Geol. Soc. 158, 969-981.

Hessami, K., Nilforoushan, F., Talbot, C.J., 2006. Active deformation within the Zagros Mountains deduced from GPS measurements. J. Geol. Soc. 163, 143-148.

Hessami, K., Pantosti, D., Tabassi, H., Shabanian, E., Abbassi, M., Feghhi, K., Solaymani, S., 2003. Paleoearthquakes and slip rates of the North Tabriz Fault, NW Iran: preliminary results. Annals Of Geophysics 46, 903-915.

Hubert-Ferrari, A., King, G., Manighetti, I., Armijo, R., Meyer, B., Tapponnier, P., 2003. Long-term elasticity in the continental lithosphere; modelling the Aden Ridge propagation and the Anatolian extrusion process. Geophysical Journal International 153.111-132.

lsacks, B., Oliver, J., Sykes, L.R., 1968. Seismology and the New Global Tectonics. J. Geophys. Res. 73, 5855-5899.

Jackson, J., 1992. Partitioning of strike-slip and convergent motion between Eurasia and Arabia in Eastern Turkey and the Caucasus. J. Geophys. Res. 97, 12471-12479.

Jackson, J., Bouchon, M., Fielding, E., Funning, G., Ghorashi, M., Hatzfeld, D., Nazari, H., Parsons, B., Priestley, K., Talebian, M., Tatar, M., Walker, R., Wright, T., 2006. Seismotectonic, rupture process, and earthquake-hazard aspects of the 2003 December 26 Bam, Iran, earthquake. Geophysical Journal International 166, 1270-1292.

Jackson, J., Haines, J., Holt, W., 1995. The accommodation of Arabia-Eurasia plate convergence in Iran. J. Geophys. Res. 100, 15205-15219.

Jackson, J., McKenzie, D., 1984. Active tectonics of the Alpine—Himalayan Belt between western Turkey and Pakistan. Geophysical Journal of the Royal Astronomical Society 77, 185-264.

Jackson, J., McKenzie, D., 1988. The relationship between plate motions and seismic moment tensors, and the rates of active deformation in the Mediterranean and Middle East. Geophysical Journal 93, 45-73.

Kadinsky-Cade, K., Barazangi, M., 1982. Seismotectonics of southern | ran: The Oman Line. Tectonics 1, 389-412.

Kostrov, V., 1974. Seismic moment and energy of earthquakes, and seismic flow of rock. Physics of the Solid Earth 1, 13-21.

Masson, F., Anvari, M., Djamour, Y., Walpersdorf, A., Tavakoli, F., Daigničres, M., Nankali, H., Van Gorp, S., 2007. Large-scale velocity field and strain tensor in Iran inferred from GPS measurements: new insight for the present-day deformation pattern within NE Iran. Geophysical Journal International 170, 436-440.

Masson, F., Chéry, J., Hatzfeld, D., Martinod, J., Vernant, P., Tavakoli, F., Ghafory-Ashtiani, M., 2005. Seismic versus aseismic deformation in Iran inferred from earthquakes and geodetic data. Geophysical Journal International 160, 217-226.

Masson, F., Djamour, Y., Van Gorp, S., Chéry, J., Tatar, M., Tavakoli, F., Nankali, H., Vernant, P., 2006. Extension in NW Iran driven by the motion of the South Caspian Basin. Earth and Planetary Science Letters 252, 180-188.

McClusky, S., Balassanian, S., Barka, A., Demir, C., Ergintav, S., Georgiev, I., Gurkan, O., Hamburger, M., Hurst, K., Kahle, H., Kastens, K., Kekelidze, G., King, R., Kotzev, V., Lenk, O., Mahmoud, S., Mishin, A., Nadariya, M., Ouzounis, A., Paradissis, D., Peter, Y., Prilepin, M., Reilinger, R., Sanli, I., Seeger, H., Tealeb, A., Toksöz, M.N., Veis, G., 2000. Global Positioning System constraints on plate kinematics and dynamics in the eastern Mediterranean and Caucasus. J. Geophys. Res. 105, 5695-5719.

McClusky, S., Reilinger, R., Mahmoud, S., Ben Sari, D., Tealeb, A., 2003. GPS constraints on Africa (Nubia) and Arabia plate motions. Geophysical Journal International 155, 126-138.

McClusky, S.C., Bjornstad, S.C., Hager, B.H., King, R.W., Meade, B.J., Miller, M.M., Monastero, F.C., Souter, B.J., 2001. Present day kinematics of the eastern California shear zone from a geodetically constrained block model. Geophysical Research Letters 28.

McKenzie, D.P., 1970. Plate Tectonics of the Mediterranean Region. Nature 226, 239-243.

Meade, B.J., Hager, B.H., 2005. Block models of crustal motion in southern California constrained by GPS measurements. J. Geophys. Res. 110, B03403.

Meade, B.J., Hager, B.H., McClusky, S.C., Reilinger, R.E., Ergintav, S., Lenk, O., Barka, A., Ozener, H., 2002. Estimates of Seismic Potential in the Marmara Sea Region from Block Models of Secular Deformation Constrained by Global Positioning System Measurements. Bulletin of the Seismological Society of America 92, 208-215.

Molnar, P., Tapponnier, P., 1975. Cenozoic Tectonics of Asia: Effects of a Continental Collision. Science 189, 419-426.

Nankali, H.R., 2011. Slip rate of the Kazerun Fault and Main Recent Fault (Zagros, Iran) from 3D mechanical modeling. Journal of Asian Earth Sciences 41, 89-98.

Nilforoushan, F., Masson, F., Vernant, P., Vigny, C., Martinod, J., Abbassi, M., Nankali, H., Hatzfeld, D., Bayer, R., Tavakoli, F.,

Ashtiani, A., Doerflinger, E., Daignières, M., Collard, P., Chéry, J., 2003. GPS network monitors the Arabia-Eurasia collision deformation in Iran. Journal of Geodesy 77, 411-422.

Nowroozi, A.A., Mohajer-Ashjai, A., 1985. Fault movements and tectonics of eastern Iran: boundaries of the Lut plate. Geophysical Journal of the Royal Astronomical Society 83, 215-237.

Okada, Y., 1985. Surface deformation due to shear and tensile faults in a half-space. Bulletin of the Seismological Society of America 75, 1135-1154.

Peyret, M., Djamour, Y., Hessami, K., Regard, V., Bellier, O., Vernant, P., Daigničres, M., Nankali, H., Van Gorp, S., Goudarzi, M., Chéry, J., Bayer, R., Rigoulay, M., 2009. Present-day strain distribution across the Minab-Zendan-Palami fault system from dense GPS transects. Geophysical Journal International 179, 751-762.

Reilinger, R., McClusky, S., Vernant, P., Lawrence, S., Ergintav, S., Cakmak, R., Ozener, H., Kadirov, F., Guliev, I., Stepanyan, R., Nadariya, M., Hahubia, G., Mahmoud, S., Sakr, K., ArRajehi, A., Paradissis, D., Al-Aydrus, A., Prilepin, M., Guseva, T., Evren, E., Dmitrotsa, A., Filikov, S.V., Gomez, F., Al-Ghazzi, R., Karam, G., 2006. GPS constraints on continental deformation in the Africa-Arabia-Eurasia continental collision zone and implications for the dynamics of plate interactions. J. Geophys. Res. 111, 805411.

Savage, J., Burford, R., 1973. Geodetic Determination of Relative Plate Motion in Central California. J. Geophys. Res. 78, 832-845. Smith, W.H.F., Wessel, P., 1990. Gridding with continuous curvature splines in tension. Geophysics 55, 293-305.

Stocklin, J., 1968. Structural history and tectonics of Iran; a review. AAPG Bulletin 52, 1229-1258.

Talebian, M., Jackson, J., 2002. Offset on the Main Recent Fault of NW Iran and implications for the late Cenozoic tectonics of the Arabia—Eurasia collision zone. Geophysical Journal International 150, 422-439.

Tavakoli, F., Walpersdorf, A., Authemayou, C., Nankali, H.R.,

Hatzfeld, D., Tatar, M., Djamour, Y., Nilforoushan, F., Cotte, N., 2008. Distribution of the right-lateral strike-slip motion from the Main Recent Fault to the Kazerun Fault System (Zagros, Iran): Evidence from present-day GPS velocities. Earth and Planetary Science Letters 275, 342-347.

Tirrul, R., Bell, I.R., Griffis, R.J., Camp, V.E., 1983. The Sistan suture zone of eastern Iran. Geological Society of America Bulletin 94, 134-150.

Vernant, P., Chéry, J., 2006. Low fault friction in Iran implies localized deformation for the Arabia-Eurasia collision zone. Earth and Planetary Science Letters 246, 197-206.

Vernant, P., Nilforoushan, F., Chéry, J., Bayer, R., Djamour, Y., Masson, F., Nankali, H., Ritz, J.F., Sedighi, M., Tavakoli, F., 2004a. Deciphering oblique shortening of central Alborz in Iran using geodetic data. Earth and Planetary Science Letters 223, 177-185.

Vernant, P., Nilforoushan, F., Hatzfeld, D., Abbassi, M.R., Vigny, C., Masson, F., Nankali, H., Martinod, J., Ashtiani, A., Bayer, R., Tavakoli, F., Chéry, J., 2004b. Present-day crustal deformation and plate kinematics in the Middle East constrained by GPS measurements in Iran and northern Oman. Geophysical Journal International 157, 381-398.

Walker, R., Jackson, J., 2002. Offset and evolution of the Gowk fault, S.E. Iran: a major intra-continental strike-slip system. Journal of Structural Geology 24, 1677-1698.

Walker, R., Jackson, J., 2004. Active tectonics and late Cenozoic strain distribution in central and eastern Iran. Tectonics 23, TC5010.

Walpersdorf, A., Hatzfeld, D., Nankali, H., Tavakoli, F., Nilforoushan, F., Tatar, M., Vernant, P., Chéry, J., Masson, F., 2006. Difference in the GPS deformation pattern of North and Central Zagros (Iran). Geophysical Journal International 167, 1077-1088.

